Received: 28 May 2024 | Revised: 14 June 2024 | Accepted: 26 November 2024

DOI: 10.1002/mawe.202300134

ARTICLE

WILEY VCH

Modeling of arcs with binary gas mixtures in a multi-arc plasma generator

Lichtbogenmodellierung in einem Multielektroden-Plasmagenerator mit binären Gasgemischen

K. Bobzin[1] | H. Heinemann[1] | M. Erck[1] | S. Warkentin[2] | O. Mokrov[2] | R. Sharma[2] | U. Reisgen[2] | K. Jasutyn[1]

[1]Surface Engineering Institute (IOT), RWTH Aachen University, Aachen, Germany

[2]Welding and Joining Institute (ISF), RWTH Aachen University, Aachen, Germany

Correspondence
K. Jasutyn, Surface Engineering Institute (IOT), RWTH Aachen University, Kackertstraße 15, 52072 Aachen, Germany.
Email: jasutyn@iot.rwth-aachen.de

Funding information
RWTH Aachen University, Grant/Award Number: SFB1120-236616214; Deutsche Forschungsgemeinschaft e.V. (DFG, German Research Foundation)

Abstract

Using plasma as an energy source in thermal spraying allows the processing of feedstock materials with high melting temperatures. In plasma spraying, hydrogen or nitrogen is commonly injected into the argon plasma, which increases the specific enthalpy and thermal conductivity. The objective of this study is to improve the understanding of this process through numerical simulation and to investigate the impact on the plasma properties. A comprehensive modelling approach for the electrodes in the three-cathode plasma generator is built upon the previous work of the authors. The plasma is described as an electromagnetically reactive fluid in local thermodynamic equilibrium using temperature-dependent thermodynamic and transport properties. The increase of flow temperature and velocity as well as the temperature distribution at the electrodes can be successfully simulated. The simulation model could accelerate parameter development for new coating systems in the future. This study completes the simulation model for multi-arc plasma spraying using binary gas mixtures.

KEYWORDS
argon-hydrogen, argon-nitrogen, atmospheric plasma spraying, computational fluid dynamics, multi-arc spraying

Abstract

Plasma als Energiequelle beim Thermischen Spritzen ermöglicht die Verarbeitung von Spritzzusatzwerkstoffen mit hohen Schmelztemperaturen. Beim Plasmaspritzen wird üblicherweise Wasserstoff oder Stickstoff als Sekundärgas in das Primärgas Argon zur Erhöhung der spezifischen Enthalpie und der Wärmeleitfähigkeit eingebracht. Ziel dieser Studie ist es, das Prozessverständnis durch numerische Simulationen zu verbessern und seine Auswirkungen

auf die Plasmaeigenschaften zu untersuchen. Ein umfassender Modellierungsansatz für die Elektroden im Drei-Kathoden-Plasmagenerator baut auf den bisherigen Arbeiten auf. Das Plasma wird als elektromagnetisch reaktives Fluid im lokalen thermodynamischen Gleichgewicht unter Verwendung der temperaturabhängigen Transporteigenschaften beschrieben. Der Anstieg der Strömungstemperatur und -geschwindigkeit sowie die Temperatur-verteilung an den Elektroden können erfolgreich simuliert werden. Das Simulationsmodell könnte in Zukunft die Entwicklung von Parametern für neue Beschichtungssysteme beschleunigen. Diese Studie vervollständigt das Simulationsmodell für das Multielektroden-Plasmaspritzen durch die Erweiterung mit binären Gasgemischen.

SCHLÜSSELWÖRTER
Argon-Stickstoff, Argon-Wasserstoff, atmosphärisches Plasmaspritzen, Multielektroden-Plasmaspritzen, numerische Strömungssimulation

1 | INTRODUCTION

Plasma spraying is a highly versatile technique for the application of protective coatings. The processing medium takes the form of a plasma, which is characterized by a high energy density ranging from $10^6\,\mathrm{J\,m^{-3}} \leq x \leq 10^7\,\mathrm{J\,m^{-3}}$, as well as a high heat flux ranging from $10^7\,\mathrm{W\,m^{-2}} \leq x \leq 10^9\,\mathrm{W\,m^{-2}}$ [1]. High heat flux of the plasma in the free jet leads to high heat transfer from the plasma to the particles, which makes plasma spraying suitable for the deposition of ceramics. Early designs of plasma torches, such as non-cascaded single cathode plasma torch, have been associated with inherent challenges during operation, including arc instability and electrode erosion [2]. Recent commercial plasma torch designs, such as multi-electrodes plasma torch, have incorporated cascaded anode and multi-electrodes to limit the movement of the arc attachment at the anode and reduce thermal load on the electrodes [3]. Multi-arc spraying promises an increase in deposition efficiencies, longer electrode life times and a wider process window, which have already been reported [2]. Two key spray gun variables, input power and net power, have been identified to correlate with the in-flight particle characteristics. Commercial plasma spray consoles make it possible to measure and control these variables easily. Adjusting the input current or secondary gas, such as hydrogen flow, can effectively compensate for any drift in the input power.

Molecular gases, primarily nitrogen and hydrogen, are commonly utilized as secondary gas to achieve plasma jets with increased enthalpy and/or velocity, thereby ensuring a higher deposition rate. One such widely used mixture is argon-hydrogen, which provides the injected particles with a high momentum through argon gas and a high heat transfer through hydrogen gas. This mixture is employed in both experimental and industrial settings, including plasma spraying. Particle heating in plasma is determined not only by plasma enthalpy but also by the thermal conductivity of the plasma gas, which can be increased by the presence of hydrogen or nitrogen in the plasma. Research has shown that the surface temperature of alumina particles injected to the argon-hydrogen plasma with 18.5 vol% hydrogen is 10% higher than other mixtures [4]. This is owing to the higher mean thermal conductivity as a result of the dissociation of hydrogen [5].

1.1 | Related works

The development of a consistent and self-sufficient simulation for the operation of a non-transferred arc plasma torch has been a challenging task. While numerical simulation is complicated and time-consuming, it is currently the only means to investigate the processes occurring within commercial plasma torches.

In modeling plasma, the electric arc model is often preferred over the kinetic plasma model due to its significantly lower computational cost [6]. By taking into account different temperatures for electrons and heavy species in a thermodynamic non-equilibrium state, known as two-temperature models, the accuracy of the electric arc model in predicting arc current density and plasma temperature is improved [7]. Furthermore, this model is also able to predict the electric arc voltage and arc behavior inside the torch [8]. This approach has been intensively utilized in the field of single-arc technology.

Recently, a comparison of prediction of anode arc attachment by local thermodynamic equilibrium and two-temperature model in a plasma torch with a single cathode and a cascaded anode was investigated. It shows that the local thermodynamic equilibrium model predicted a constricted anode arc attachment that moves on the anode ring, while the two-temperature model predicted a diffuse and steady arc attachment with a better prediction of the actual voltage compared to the measured arc voltage [9]. Moreover, the inclusion of the cathode sheath model in the two-temperature magnetohydrodynamic model results more reliable prediction of the torch voltage and cooling loss [10]. Intensive research and progress in the field of modeling the single-arc plasma spraying, including both conventional and cascaded arc techniques, have helped to achieve a better understanding of the process. However, the potential benefits of multi-arc spraying have not been fully explored through numerical simulations, which could provide insight into its limits and possibilities. In comparison to single-arc plasma spraying, where the complexity of the arc fluctuations in the process limits the predictive power of numerical models, the positions of the arcs in the torch do not change significantly in multi-arc plasma spraying. This enables a numerical analysis of the multi-arc plasma process using an local thermodynamic equilibrium approach, which provides better predictive power for the simulations in terms of calculated velocities and temperatures with a steady-state analysis. The local thermodynamic equilibrium approach is supported by a user-defined subroutine that is implemented as a temperature- and pressure-dependent net energy term in the energy conservation equation. In this study, radiation is treated with the net emission coefficient model. In this study and current project, a three-cathode plasma torch is further investigated to extend the simulation chain of atmospheric plasma spraying. The simulation chain consists of plasma generator simulation, free jet model with particle injection, particle impact and coating build-up simulation, with the aim of predicting the effective coating properties such as thermal conductivity of thermally sprayed coatings. In previous works, numerical study of three-cathode cascaded plasma torch with different operating conditions using argon as plasma gas has been developed [11]. By means of advanced computer tomography which allows a three-dimensional reconstruction of plasma jet, the numerical results were validated [12]. A comprehensive analysis was conducted to investigate the impact of the operating gas on the flow characteristics of the plasma torch's predecessor model [13]. Following that, the model was applied to the latest generation of the three-cathode plasma torch to conduct a numerical study of the pure argon plasma processing conditions [14].

The potential of hydrogen and nitrogen as secondary gases has not been thoroughly explored through numerical simulations. This study aims to expand the existing simulation process chain of plasma spraying using a three-cathode torch with binary gas composition, and analyze the impact of nitrogen and hydrogen as secondary gases on plasma properties and electrodes. The simulation model is further developed by discretizing the electrodes to determine the temperature of the electrodes in various process parameters.

2 | MODEL DESCRIPTION

This study investigates three cathodes plasma spray gun TriplexPro-210 with 9 mm nozzle diameter. The simulation model is built upon the work [14]. The plasma is characterized as an electromagnetically reactive fluid in local thermodynamic equilibrium with temperature-dependent thermodynamic and transport properties. The model considers the conservation equations for mass, momentum, and enthalpy, which are coupled with the electromagnetic field equations to describe the magnetohydrodynamic flow. Turbulence is taken into account and modelled with shear stress transport turbulence model. Due to the high temperatures, radiation within the plasma spray gun cannot be neglected, and it is treated using the net emission coefficient model.

The simulation model can be expressed by the following system of equations:

$$\frac{\partial \rho}{\partial t} + \nabla \cdot (\rho\, \vec{u}) = 0 \tag{1}$$

$$\rho\left(\frac{\partial \vec{u}}{\partial t} + \vec{u} \cdot \nabla \vec{u}\right) = \rho\, \vec{g} + \nabla \cdot \vec{\tau} - \nabla p + \vec{f}_L \tag{2}$$

$$\frac{\partial \rho\, h}{\partial t} + \nabla \cdot (\rho\, h\, \vec{u}) = \nabla \cdot \left(\frac{\lambda}{c_p} \nabla h\right) + S_{Joule} + S_{Net} \tag{3}$$

where t is the time, ρ gas density, $\vec{u}$ gas velocity, p pressure, $\vec{g}$ gravitation, $\vec{\tau}$ stress tensor, h gas enthalpy, λ thermal conductivity, and c_p specific heat at constant pressure. These three equations belong to the conservation equations for mass, momentum, and enthalpy.

The magnetohydrodynamics are covered by the conductive media approximation as described in Ansys CFX theory guide. The potential formulation is:

$$\vec{E} = -\vec{\nabla}\varphi \tag{4}$$

as the electric potential φ for electric field $\vec{E}$ and:

$$\vec{B} = \nabla \times \vec{A} \tag{5}$$

as the magnetic vector potential $\vec{A}$ for magnetic induction $\vec{B}$. The continuity equation for the electric current for a stationary case is defined as:

$$\nabla \ <M.> \vec{j} \ = 0 \tag{6}$$

and as a constitutive relationship, the current density can be written as:

$$\vec{j} = \ \sigma \ (\vec{E} + \vec{u} \times \ \vec{B}) \tag{7}$$

Using the equation (5) and the Ampère's law, the transport equation for the magnetic vector potential is as follows:

$$\nabla <M.> (\overrightarrow{\frac{1}{\mu_0} \nabla A}) = \ \sigma \ (\vec{E} + \vec{u} \times (\nabla \times \ \vec{A})) \tag{8}$$

Here, σ represents the electrical conductivity and μ_0 stands for the permeability of vacuum.

The influence of the electromagnetic field on the fluid dynamics is described by the Lorentz force $\vec{\mathbf{f}}_{\mathbf{L}}$: 9

$$\overrightarrow{f_L} = \vec{j} \ \times \ \vec{B} \tag{9}$$

Joule heating S_{Joule} is described by:

$$S_{Joule} = \vec{j} \ <M.> \ (\vec{E} + \vec{u} \ \times \ \vec{B}) \tag{10}$$

This term provides resistive heating of the gas and completes the conservation of enthalpy equation (3).

Due to the very high plasma temperatures inside the plasma torch, radiation losses cannot be neglected. In addition, the reflection at the nozzle walls is responsible for the reabsorption of fluid energy. In the present study, the net radiative flux is calculated by multiplying the net emission coefficients [15], by 4π. Although it cannot be ruled out that the thickness of the plasma column does not change along the plasma chamber, the radiation flux is approximated with a constant characteristic length of radius of 1 mm. The net radiative flux is described by a temperature-dependent net energy term S_{Net}, which takes into account the radiation and the reabsorption of energy.

The calculations are performed in parallel on multiprocessor workstations using 24 computation cores of a high-performance cluster equipped with processor model Intel® Xeon® Gold 6258R with the commercial computational fluid dynamics software package ANSYS CFX Release 21.2. The computation time required to solve each simulation was about 8 hours.

2.1 | Simulation domain

The three-cathode plasma spray gun is threefold rotationally symmetric, which is utilized by using a one-third section of the geometry as the calculation domain, Figure 1. Rotational periodic boundary conditions are defined at the cutting planes, which intersect each other at an angle of $\alpha = 120°$. The assumption of rotational symmetry is based on the conservation of physical quantities. In the case of the electromagnetic field, the laws of electromagnetism, which are described by Maxwell equations, ensure that the behavior of the magnetic field is consistent across the rotation axis [16]. The entire geometry is used as the calculation area by defining

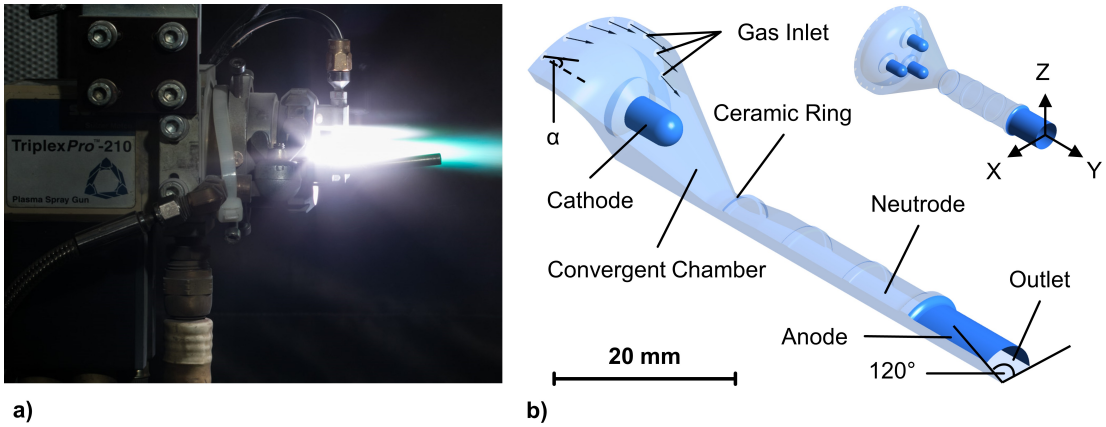

FIGURE 1 Multi-arc plasma torch: a) TriplexPro-210 and b) Simulation domain.

BILD 1 Multielektroden-Plasmabrenner: a) TriplexPro-210 and b) Simulationsdomäne.

periodic boundary conditions on the section planes. The simulation model consists of a fluid domain for the gas flow and solid domains for the cathodes and anode. Plasma gas is fed through 24 inlets with an inclination angle of 25° into the convergent chamber where three water-cooled cathodes are placed. The plasma gas then flows through a long tubular section with a neutrode block and then continues through the anode ring, which is located next to the nozzle outlet.

The simulations and subsequent experiments are conducted using the following gas mixtures while maintaining a constant electrical current of $I = 450$ A and a total gas flow of $V_G = 69$ SLPM, Table 1. The current is then distributed evenly among three cathodes. The process parameters using binary gas mixtures have been carefully selected to facilitate the examination of practical process conditions. In order to ensure a straightforward comparison, the volume flow rate of pure argon as the plasma gas is maintained at the same level as that used in the binary gas mixtures.

2.2 | Boundary conditions

The volumetric flow rate is used to regulate the plasma gas flow in the plasma spraying system. Based on the known densities of the plasma gas, the mass flow rates are calculated and utilized as inflow boundary conditions for the simulation. Typically, plasma gas is introduced into the chamber at an angle resulting from the arrangement and inclination of the feeding pipes. However, to optimize calculation costs and element quality, the feeding pipes are not included in the calculation domain. Instead, the flow direction of the incoming gas is represented by applying the flow direction on the inlet boundary condition. The outflow boundary condition with atmospheric pressure is set at the nozzle outlet. Zero flux boundary condition is imposed for electric potential at the inflow and the components of magnetic vector potential are set to zero.

The walls of the plasma chamber such as neutrode, ceramic rings and housing are defined as non-conducting walls with zero flux boundary condition for electric potential. The temperature of the walls can be assumed to be constant with a static wall temperature of $T = 500$ K. The magnetic potential of the walls is set to zero.

The complexity of configuring boundary conditions at the electrodes can vary depending on the simulation's purpose and the physics and scales being resolved by the implemented models. If the goal is to determine possibility of electrode erosion through numerical methods, precise calculation of heat transfer onto the electrodes is necessary. This requires discretization of the anode and cathodes to account for heat transfer resulting from the surrounding plasma and arc attachment. An electrical potential value of $U = 0$ V is assigned to the outer surface of the solid calculation domain of anode. The plasma gun is cooled with water flow of up to 25 litre per minute. Using this information and the monitored water temperature as it enters and exits the cooling circuit, the heat exchange between the anode and the cooling water can be modeled. Based on the monitored volume flow rate of water, water temperature and area of the surface of the cooled anode and cathodes, heat flux can be calculated and thus with the difference of inflowing and outflowing water temperature and assumption of the wall temperature of the copper of $T = 500$ K, the heat transfer coefficient can be calculated. To account the heat transfer to the anode, a heat transfer coefficient of $h = 2.14 \cdot 10^4$ W m^{-2} K^{-1}, $h = 3.17 \cdot 10^4$ W m^{-2} K^{-1} $h = 2.96 \cdot 10^4$ W m^{-2} K^{-1} is determined from the corresponding monitored water temperature as the outer anode temperature with temperature of $T = 304$ K, $T = 309$°K, $T = 309$ K for the parameter with pure argon, argon-hydrogen, and argon-nitrogen gases, respectively. Since this model relies on local thermodynamic equilibrium approximation, substantial heating by the electrons absorbed by the anode is not taken into consideration. The material properties of both the tungsten cathode and anode are temperature-dependent. The tungsten material properties were taken from [17]. The total amount of electric current flowing into the calculation domain is defined by assigning a uniform electric current density

TABLE 1 Volume content of the operating gases investigated and corresponding total mass flow rate.Volume content of the operating gases investigated and corresponding total mass flow rate.

TABELLE 1 Volumenstrom der untersuchten Prozessgase und entsprechender Gesamtmassendurchsatz.

Parameter	Argon	Hydrogen	Nitrogen	Mass flow rate
Argon	69 SLPM	–	–	0.00205 kg/s
Argon-hydrogen	60 SLPM	9 SLPM	–	0.00180 kg/s
Argon-nitrogen	60 SLPM	–	9 SLPM	0.00197 kg/s

perpendicular to the outer surface of the cathode domain. A heat transfer coefficient, as described in the paragraph above, is also applied to the cathode base for consideration of the cooling effect by the water. In summary, the pressure p, velocity $\vec{u}$, temperature T, electric potential φ, and magnetic vector potential $\vec{A}$are each defined at the boundaries, Table 2.

A heat source is implemented near the electrodes for the ignition of the arc for first few iterations [18]. The temperature of the plasma gas is heated up to $T=$ 12,000 K and then the current is introduced at the cathodes. An artificial electrical conductivity to the elements located near the anode surface is not assigned to minimize the effect of unrealistic arc attachment. The simulation model does not consider the coupling of the plasma with both electrodes through the sheath process. Nevertheless, a conservative heat flux and the heat loss due to the water cooling at the anode and the cathode base are modeled.

2.3 | Gas properties

The accuracy of the simulation results heavily relies on the use of appropriate thermodynamic and transport properties for the operating gas. In the present study, the thermodynamic and transport properties of pure argon, a mixture of 87% argon and 13% nitrogen, and a mixture of 87% argon and 13% hydrogen are sourced from the work [19–21], Figure 2. The percentage of the binary gas mixtures is based on mole fraction ratio. The pressure dependency of the thermodynamic and transport properties of the plasma gas at 50 kPa, 100 kPa, 200 kPa, 500 kPa, and 1000 kPa is considered, Figure 3.

3 | RESULTS AND DISCUSSION

Thermal efficiencies of the torch, which is defined as the ratio of the output power of the plasma jet to the input power, are calculated for different gas compositions. In order to calculate the electrical input power, first of all the resulting voltages for different runs are calculated. Through multiplication of the resulting voltages by $I=$ 450 A of operating electrical current, input powers of the electric supply are calculated. The power output at the torch outlet is derived directly from the simulation results by calculating the product of plasma enthalpy and mass flow, Table 3. The thermal efficiency is determined

TABLE 2 Boundary conditions used in the simulation setup.

TABELLE 2 Verwendete Randbedingungen in der Simulation.

Boundary	p (Pa)	$\vec{u}$ (m s^{-1})	T (K)	φ (V)	$\vec{A}$ (Vs m^{-1})
Inlet	$p(\dot{m}_i)$	$\vec{u}(\dot{m}_i)$	300	$\frac{\partial\varphi}{\partial n}=0$	$\vec{A}=0$
Convergent chamber, ceramic ring, neutrode	$\frac{\partial p}{\partial n}=0$	$\vec{u}=0$	500	$\frac{\partial\varphi}{\partial n}=0$	$\vec{A}=0$
Cathode wall	$\frac{\partial p}{\partial n}=0$	$\vec{u}=0$	500	$j(A)$	$\vec{A}=0$
Anode wall	$\frac{\partial p}{\partial n}=0$	$\vec{u}=0$	500	$\varphi=0$	$\vec{A}=0$
Outlet	$\frac{\partial p}{\partial n}=0$	$\frac{\partial\vec{u}}{\partial n}=0$	$\frac{\partial T}{\partial n}=0$	$\frac{\partial\varphi}{\partial n}=0$	$\vec{A}=0$

TABLE 3 Thermal efficiencies, voltages, cooling losses, input and output powers of the torch for different process parameters.

TABELLE 3 Thermische Wirkungsgrade, Spannungen, Kühlleistungen, elektrische- und Wirkleistungen des Plasmabrenners für verschiedene Prozessparameter.

Parameter	Argon	Argon-hydrogen	Argon-nitrogen
Measured values			
Current	450 A	450 A	450 A
Voltage	99 V	121 V	122 V
Electrical input power	44.6 kW	54.7 kW	54.6 kW
Cooling loss	16.7 kW	24.1 kW	22.5 kW
Output power	27.9 kW	30.6 kW	32.1 kW
Thermal efficiency	0.63	0.56	0.59
Simulated values			
Current	450 A	450 A	450 A
Voltage	98 V	134 V	123 V
Electrical input power	44.2 kW	60.1 kW	55.3 kW
Output power based on enthalpy and mass flow rate	32.3 kW	42.5 kW	37.2 kW
Thermal efficiency	0.73	0.71	0.67

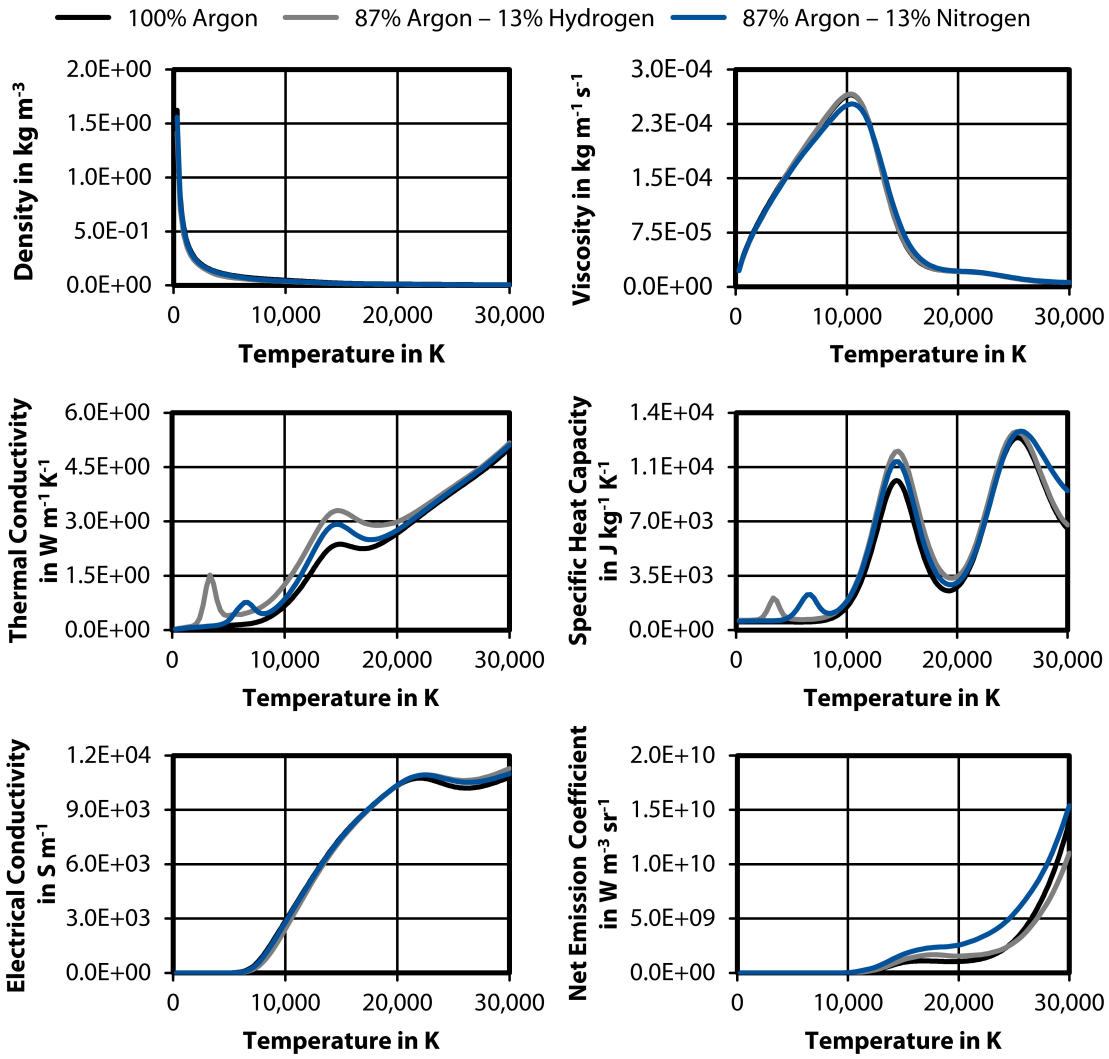

FIGURE 2 Thermodynamic and transport properties of the gas mixtures argon, argon-hydrogen, and argon-nitrogen.

BILD 2 Thermodynamische und Transporteigenschaften der Gasgemische Argon, Argon-Wasserstoff und Argon-Stickstoff.

by dividing the output power by the input power. This output power, also regarded as net power, is determined by subtracting the electrical input power from the cooling loss. These values are added into Table 3 for comparison.

The voltages between the individual cathodes and the anode were measured for each set of parameters studied. The voltage value was the average of the individual values of the measured voltages per cathode, Table 3, Figure 4. The simulation results for the voltage were in good conformity with the experimental measurements, with an overestimation of just over 1% observed for pure argon, around 11% for argon-hydrogen and slightly under 1% for argon-nitrogen mixtures. Both simulation and experimental results show that the use of hydrogen and nitrogen as secondary gas increases the electric potential. The output power, also referred to as net power, is determined by multiplying the mass flow rate of the plasma gas by its specific enthalpy. In the case of binary gas mixtures, the output power tends to be higher compared to pure argon.

3.1 | Effect of secondary gas on the electrodes

Understanding the behavior at the electrodes during plasma spraying is critical for improving the efficiency and quality of the process. This study was conducted to give an insight how various process parameters affect electrode temperature and current density. The study revealed that the maximum temperature of the cathodes occurred near the edge rather than at the tip, due to the swirling flow of gas in the plasma gun chamber before entering the neutrode, Figure 5. The arc is dragged along by the vortex gas flow, which causes a corresponding

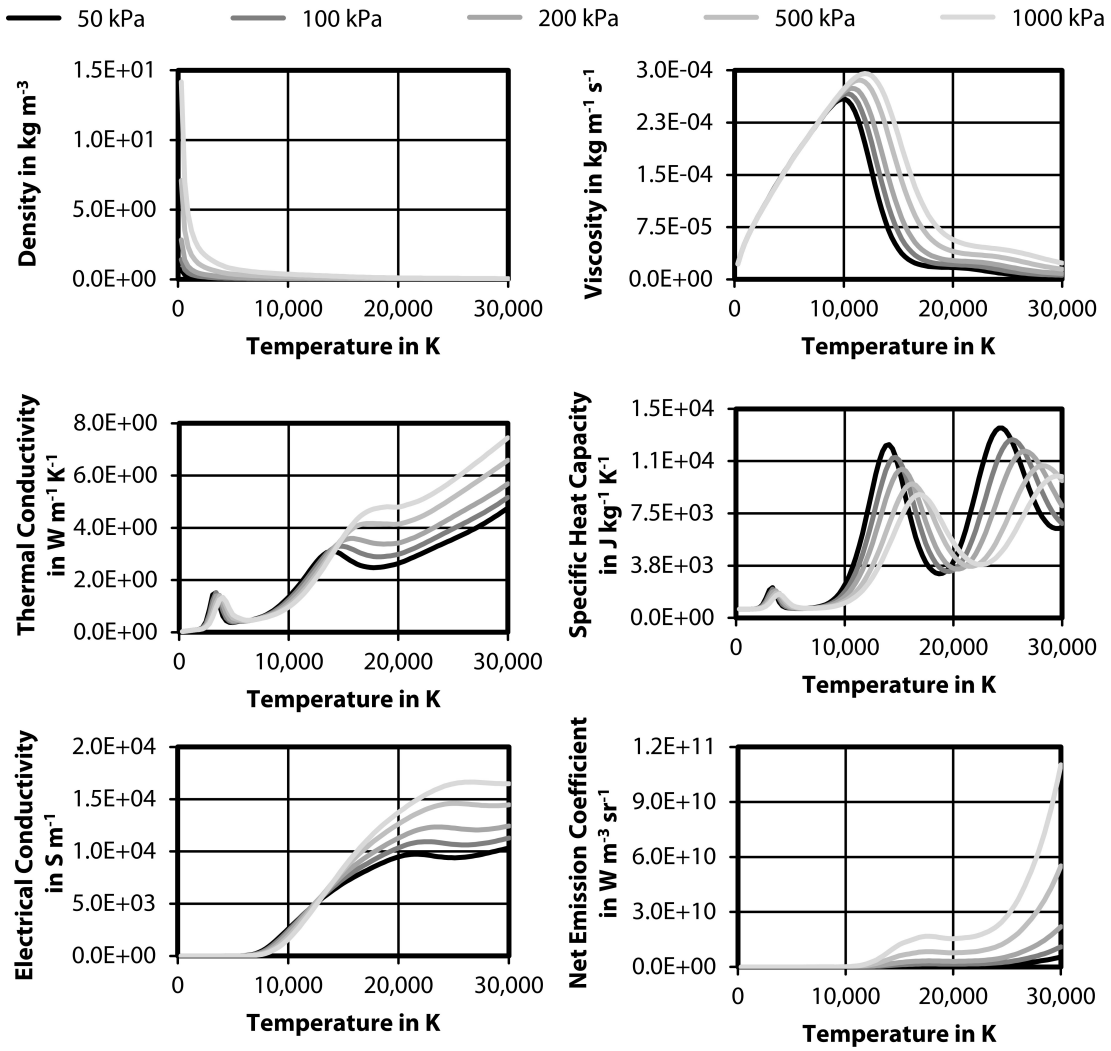

FIGURE 3 Thermodynamic and transport properties of the gas mixture argon-hydrogen as a function of pressure.

BILD 3 Thermodynamische und Transporteigenschaften des Gasgemisches Argon-Wasserstoff in Abhängigkeit vom Druck.

rotation and angular displacement of the arc cores relative to the cathodes. The use of hydrogen as the secondary gas resulted in the highest temperature of $T=$ 3,803 K, while pure argon and argon-nitrogen yielded temperatures of $T=2{,}713$ K and $T=3{,}288$ K, respectively. The maximum current density at the cathodes was observed at $J=4.41\cdot10^7\,\mathrm{A\,m^{-2}}$, $J=6.41\cdot10^7\,\mathrm{A\,m^{-2}}$, and $J=5.90\cdot10^7\,\mathrm{A\,m^{-2}}$ for pure argon, argon-hydrogen, and argon-nitrogen gases, respectively. The thermionic current density $\mathbf{J_{em}}$ can be calculated from the Richardson-Dushman law relating the emission to the cathode temperature $\mathbf{T_c}$ and work function $\phi_\mathbf{c}$ with $\phi_c=4.2$ eV, assuming that the cathode material is pure tungsten with neglection of Schottky effect:

$$J_{em} = \lambda_R\, A_0\, T_c^2\, exp(-\frac{e\phi_c}{k_b T_c}) \tag{11}$$

λ_R is a material-specific correction factor that is typically of order 0.5, A_0 is an empirical constant with $\mathrm{A_0}=1.2\cdot10^6\,\mathrm{A\,m^{-2}K^{-2}}$, e is the electron charge, and k_b is the Boltzmann constant. The calculated thermionic current density of the obtained cathode temperatures is $J_{em}=6.98\cdot10^4\,\mathrm{A\,m^{-2}}$, $J_{em}=2.36\cdot10^7\,\mathrm{A\,m^{-2}}$, and $J_{em}=2.37\cdot10^6\,\mathrm{A\,m^{-2}}$ for pure argon, argon-hydrogen, and argon-nitrogen gases, respectively. It is obvious that the simulated maximum cathode temperature for the case of pure argon plasma is relatively low for a thermionic emission. This current state of the numerical model needs a surrogate model introducing a heat model that accounts for the heat flux induced by the sheath processes. This includes the heat loss by the thermionic electrons and the heating caused by the ions.

An attempt was made to predict the arc attachment at the anode using surrogate modeling. However, this model does not allow an exact prediction of the arc attachment, but only serves as a basis for determining the

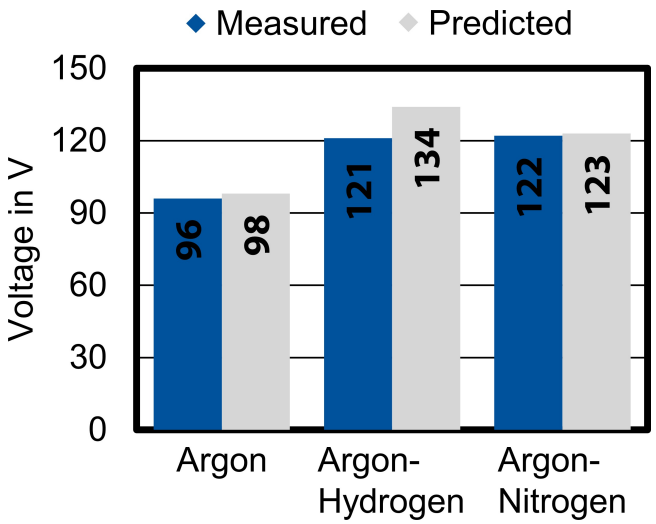

FIGURE 4 Predicted and measured voltages of investigated plasma gas mixtures.

BILD 4 Berechnete und gemessene Spannungen der untersuchten Plasmagasgemische.

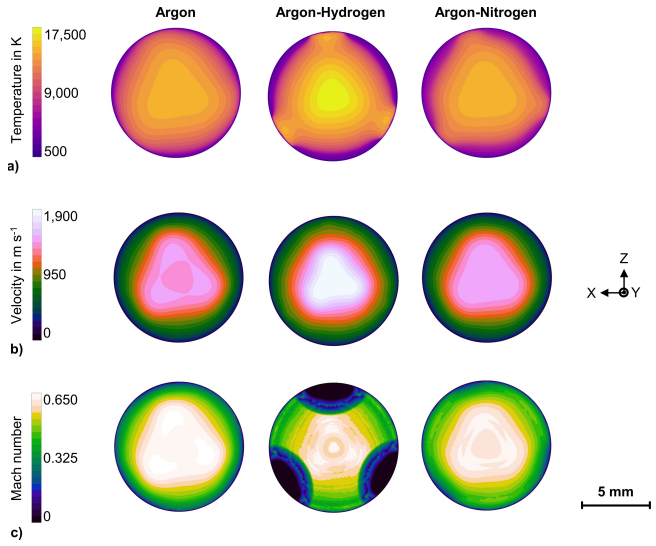

FIGURE 5 Current density distribution: a) inside the plasma torch and b) as isosurface and predicted temperature distribution under argon-hydrogen plasma on the: c) cathodes and d) anode.

BILD 5 Stromdichteverteilung: a) im Inneren des Plasmabrenners und b) als Isofläche und berechnete Temperaturverteilung bei Argon-Wasserstoff-Plasma an: c) Kathoden und d) Anode.

heat distribution on the anode. Nevertheless, the anode exhibited three hotspots that corresponded to the bridging of the arc for each cathode. The isosurface of current density $> 5 \cdot 10^6\ \mathrm{A\,m^{-2}}$ indicates the local arc attachments at the anode. The gas inlet direction of the operating gas causes an intensive fluid swirl in the converging part of the torch chamber towards the nozzle outlet. In this part of the torch, the arcs are dragged along by the swirling gas flow. As a result, the anode arc attachments are positioned at a certain angle of rotation to the cathodes. The triple anode attachment produces a triangular pattern of the plasma jet in this three-cathode plasma gun. The angle at which this triangular pattern is rotated shifts with an increase in the plasma gas flow and the plasma current. With a tripling of the gas flow, a shift of up to 60° was observed in the Triplex II, also a three-cathode plasma gun with a 9 mm nozzle, which is certainly caused by the vortex flow as reported in [22]. The anode, made of copper with tungsten on its inner surface, had lower temperatures than a pure copper anode in conventional plasma torch, with maximum temperatures of $T = 779$ K, $T = 1{,}315$ K, and $T = 898$ K observed for pure argon, argon-hydrogen, and argon-nitrogen plasma.

3.2 | Effect of secondary gas on the plasma properties

The position and geometry of the plasma column within a torch are determined by the thermodynamic and transport properties of the plasma-forming gas. The interplay between temperature-dependent properties of the gas affects the temperature and velocity distribution within the torch. To investigate the impact of various gas mixtures on the plasma properties, this study analyzed the temperatures, velocities, and Mach number distribution at the nozzle outlet, Figure 6. The results indicate that argon-hydrogen plasma produces a slight higher outlet velocity than other gas mixtures at an equivalent volume flow rate. Specifically, the calculated average velocity is 11.4% and 10.4% lower for argon and argon-nitrogen mixtures, compared to argon-hydrogen with $v = 1{,}054\ \mathrm{m\,s^{-1}}$. It can also be seen from the distribution of Mach number at the nozzle outlet that pure argon and argon-nitrogen plasma are similar in Mach number contour. The argon-hydrogen plasma shows a more constricted plasma with high kinetic energy around the center region of the nozzle outlet. The Mach number contour of the argon-hydrogen plasma at the nozzle exit wall has some very low Mach number regions, while this cannot be detected for the velocity contour. This is possibly attributed to the higher temperature in these three regions, which leads to a higher speed of sound, Figure 6a. In addition, the three higher temperature regions are the result of neglecting the artificial electrical conductivity near the anode, allowing the arcs to attach freely, in this case near the nozzle outlet. Additionally, the calculated average temperatures for these mixtures are lower, with the argon-nitrogen mixture showing the lowest values. The average temperatures at the torch outlet are approximately 3.2% and 7.8% lower for argon

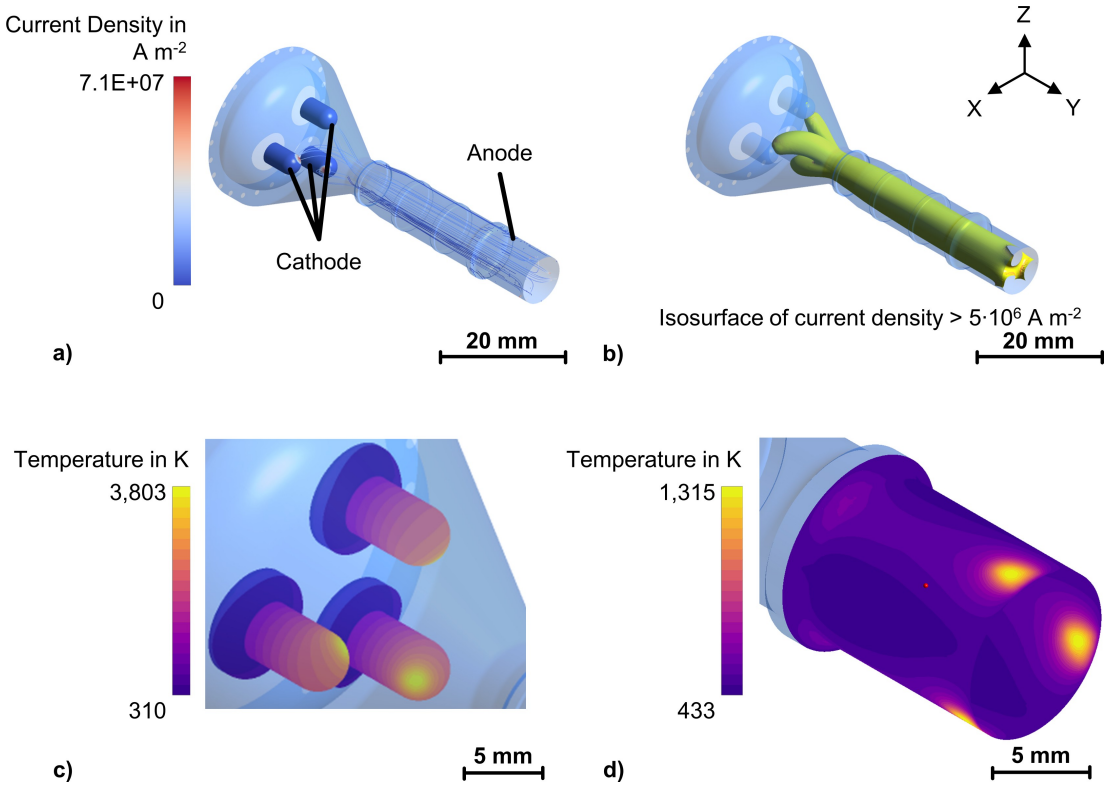

FIGURE 6 Calculated: a) temperature, b) velocity, and c) Mach number contour of pure argon, argon-hydrogen, and argon-nitrogen plasma at the nozzle outlet.

BILD 6 Berechnete: a) Temperatur-, b) Geschwindigkeitsfelder, und c) Machzahl von Plasma mit reinem Argon, Argon-Wasserstoff und Argon-Stickstoff am Düsenausgang.

and argon-nitrogen mixtures, respectively, compared to argon-hydrogen with $T = 11{,}580$ K.

It is noteworthy that the specific enthalpy of the plasma jet, in addition to thermal conductivity is a critical factor in the heat transfer to the sprayed particles [4]. The specific enthalpy represents the energy available per unit mass of the flow. The numerical calculation shows that the plasma with pure argon has a specific enthalpy of $H = 15.5\ \mathrm{MJ\,kg^{-1}}$, while the addition of hydrogen and nitrogen to the gas mixture results in higher specific enthalpy values of $H = 23.7\ \mathrm{MJ\,kg^{-1}}$ and $H = 18.9\ \mathrm{MJ\,kg^{-1}}$, respectively.

4 | CONCLUSION

A three-dimensional computational fluid dynamics model of an industrial plasma torch with three cathodes was developed using a local thermodynamic equilibrium and simplified surrogate models for arc attachment. The effects of binary gas mixtures on plasma properties, in particular at the nozzle outlet, have been numerically investigated in a three-cathode system and compared to a pure argon plasma. The obtained results are outlined below:

- The addition of hydrogen and nitrogen gases in the plasma spray system is expected to increase voltage and thus the electrical power, and this was successfully replicated through numerical simulations. The predicted voltage values from the simulations were found to be in good agreement with experimental measurements.
- The temperature distribution of the cathodes showed that the maximum temperature was located near the edge, rather than at the tip. When using a plasma gas mixture with hydrogen, both the cathode and anode temperatures were observed to be higher compared to other gas mixtures.
- In the present case, where the volume flow rate of pure argon and binary gas mixtures remained constant, the average temperature of the argon-hydrogen plasma were found to be only 3 to 8% higher than the plasma with pure argon gas and argon-nitrogen mixture. It is noteworthy that adding hydrogen and nitrogen to argon results in a higher specific enthalpy compared to pure argon. Specific enthalpy of the plasma

jet is a decisive factor for the heat transfer to the injected particles in addition to the thermal conductivity. The average velocity of argon-hydrogen is over 10% and 11% higher than pure argon and argon-nitrogen plasma.

In future work, the properties of the plasma with binary gas mixtures at the nozzle outlet will be applied to a plasma jet simulation to examine their influence on particle properties. The accuracy of the simulation model will be confirmed through the measurement of plasma temperature in the plasma jet using computer tomography. To improve the predictive capacity of this numerical model, incorporating the cathode sheath can be a valuable addition as it considers the interaction of charged particles. This inclusion facilitates the coupling at the cathode-plasma interface, resulting in a more precise calculation of heat generation and electric potential. In terms of identifying the potential wear of the anode as part of the scope of the current project, more precise modeling of the anode, including heating by the electrons, is expected in future work.

ACKNOWLEDGEMENTS

The presented investigations were carried out at RWTH Aachen University within the framework of the Collaborative Research Centre SFB1120-236616214 "Bauteilpräzision durch Beherrschung von Schmelze und Erstarrung in Produktionsprozessen" and funded by the Deutsche Forschungsgemeinschaft e.V. (DFG, German Research Foundation). The sponsorship and support are gratefully acknowledged. Simulations were performed with computing resources granted by RWTH Aachen University under project rwth0570. Open Access funding enabled and organized by Projekt DEAL.

CONFLICT OF INTEREST STATEMENT

The authors declare no financial or commercial conflict of interest.

DATA AVAILABILITY STATEMENT

The data that support the findings of this study are available from the corresponding author upon reasonable request on http://hdl.handle.net/ using the persistent identifier 21.11102/dc08370b-77a0-43b6-a538-b2170102e262.

ORCID

M. Erck http://orcid.org/0009-0004-8998-2895
R. Sharma http://orcid.org/0000-0002-6976-4530
U. Reisgen http://orcid.org/0000-0003-4920-2351
K. Jasutyn http://orcid.org/0000-0001-5816-273X

REFERENCES

1. C. Chazelas, J. P. Trelles, A. Vardelle, *J. Therm. Spray Technol.* **2017**, *26*, 3.
2. A. Vardelle, C. Moreau, N. J. Themelis, C. Chazelas, *Plasma Chem. Plasma Process.* **2015**, *35*, 491.
3. J. Schein, J. Zierhut, M. Dzulko, G. Forster, K. D. Landes, *Contrib. Plasma Phys.* **2007**, *47*, 498.
4. M. Vardelle, A. Vardelle, P. Fauchais, *J. Therm. Spray Technol.* **1993**, *2*, 79.
5. B. Pateyron, M.-F. Elchinger, G. Delluc, P. Fauchais, *Plasma Chem. Plasma Process.* **1992**, *12*, 421.
6. H. C. Kim, F. Iza, S. S. Yang, M. Radmilović-Radjenović, J. K. Lee, *J. Phys. D* **2005**, *38*, R283.
7. K. C. Hsu, E. Pfender, *J. Appl. Phys.* **1983**, *54*, 4359.
8. J. P. Trelles, J. V. R. Heberlein, E. Pfender, *J. Phys. D* **2007**, *40*, 5937.
9. R. Zhukovskii, C. Chazelas, V. Rat, A. Vardelle, R. Molz, *J. Therm. Spray Technol.* **2022**, *31*, 28.
10. R. Zhukovskii, C. Chazelas, V. Rat, A. Vardelle, R. J. Molz, *J. Therm. Spray Technol.* **2023**, *32*, 532.
11. K. Bobzin, N. Bagcivan, L. Zhao, I. Petkovic, J. Schein, K. Hartz-Behrend, S. Kirner, J.-L. Marqués, G. Forster, *Front. Mech. Eng.* **2011**, *6*, 324.
12. K. Bobzin, N. Bagcivan, I. Petkovic, *J. Mater. Process. Technol.* **2011**, *211*, 1620.
13. K. Bobzin, N. Kopp, T. Warda, M. P. Schäfer, M. Öte, presented at ITSC 2013, Busan, South Korea, May 13–May 15, **2013**, pp. 400–405.
14. K. Bobzin, M. Öte, *J. Therm. Spray Technol.* **2016**, *25*, 920.
15. J. Menart, S. Malik, *J. Phys. D* **2002**, *35*, 867.
16. M. Dreher, U. Füssel, M. Schnick, presented at the 9th International Seminar 'Numerical Analysis of Weldability', Graz, Austria, Sep 28–Sep 30, **2009**.
17. P. Tolias, *Nucl. Mater. Energy* **2017**, *13*, 42.
18. E. Moreau, C. Chazelas, G. Mariaux, A. Vardelle, *J. Therm. Spray Technol.* **2006**, *15*, 524.
19. A. B. Murphy, C. J. Arundell, *Plasma Chem. Plasma Process.* **1994**, *14*, 451.
20. A. B. Murphy, E. Tam, *J. Phys. D* **2014**, *47*, 295202.
21. A. B. Murphy, *Plasma Chem. Plasma Process.* **2000**, *20*, 279.
22. J. Schein, M. Richter, K. D. Landes, G. Forster, J. Zierhut, M. Dzulko, *J. Therm. Spray Technol.* **2008**, *17*, 338.

How to cite this article: K. Bobzin, H. Heinemann, M. Erck, S. Warkentin, O. Mokrov, R. Sharma, U. Reisgen, K. Jasutyn, *Materialwiss. Werkstofftech.* **2024**, *55*, e202300134. https://doi.org/10.1002/mawe.202300134